

# Symmetry accounting in the integral-equation analysis of lasing eigenvalue problems for two-dimensional optical microcavities

ALEXANDER O. SPIRIDONOV,<sup>1</sup> EVGENII M. KARCHEVSKII,<sup>1</sup> AND ALEXANDER I. NOSICH<sup>2,\*</sup>

<sup>1</sup>Department of Applied Mathematics, Kazan Federal University, Kazan 420008, Russia

<sup>2</sup>Laboratory of Micro and Nano Optics, Institute of Radio-Physics and Electronics NASU, Kharkiv 61085, Ukraine

\*Corresponding author: anosich@yahoo.com

Received 25 May 2017; revised 26 May 2017; accepted 26 May 2017; posted 31 May 2017 (Doc. ID 286504); published 19 June 2017

We consider the modes of two-dimensional (2D) microcavity lasers as active open dielectric resonators using the linear electromagnetic formalism of the lasing eigenvalue problem (LEP) with exact boundary and radiation conditions. We reduce LEP to a nonlinear eigenvalue problem for the Muller boundary integral equation and build a sophisticated numerical method accounting for the possible symmetry properties of sought solutions. Namely, we take into account the presence of one, two, or four lines of symmetry. This helps split solutions into independent classes, which contributes to the stability of calculations and reduces the size of the approximate matrix eigenvalue problems. © 2017 Optical Society of America

**OCIS codes:** (140.3945) Microcavities; (140.5960) Semiconductor lasers; (260.2110) Electromagnetic optics; (030.4070) Modes; (050.1755) Computational electromagnetic methods.

<https://doi.org/10.1364/JOSAB.34.001435>

## 1. INTRODUCTION

Microcavity lasers have been an object of intensive research since the 1990s, both experimentally and theoretically [1–16]. Here, most of the works on their modeling were based on the search of the complex-valued natural frequencies of passive cavities and therefore were not able to deliver the most important lasing characteristic—the threshold gain. To overcome this significant drawback, several approaches were proposed recently [17–22], including the lasing eigenvalue problem (LEP) [3,4,6,7,12,23]. LEP is a mathematical boundary-value problem based on the classical electromagnetic equations for open resonators equipped with active regions. Then the threshold value of material gain in the active region, for a given mode, can be extracted from LEP as an eigenvalue, together with the corresponding frequency of lasing.

In the case of microcavity lasers, such as semiconductor, doped-polymer, or crystalline, the task is determining the modes of a dielectric resonator, which is fully or partially filled in with a gain material. Although LEP can be combined with any numerical method (except finite differences in the time domain because such codes cannot handle eigenvalue problems directly), the most efficient approach is offered by the method of analytical regularization [24,25]. For dielectric bodies, the analytical regularization treatment means reducing the eigenvalue problem to the search for characteristic numbers of the Muller boundary integral equation (BIE) [6,7,26]. The

Muller BIE is a judicious combination of electric-field and magnetic-field integral equations (IEs) on the cavity's boundary, derived using Green's formulas in the interior and exterior domains and the dielectric-boundary conditions. This procedure cancels the strong singularities in kernel functions and yields a Fredholm IE of the second kind.

Thus the Muller BIE derivation effectively means the explicit inversion of the small-contrast part of the vector electromagnetic-field problem. The final result is a set of two or four coupled equations in the case of 2D and 3D scatterers, respectively. Further, it can be discretized in trusted way and then the eigenvalues are approximated with the roots of a determinantal equation. This is a complex-valued transcendental equation, the roots of which are usually found by a suitable combination of global search (pseudo-random) and local search (iterative) algorithms. What is important is that the convergence of the approximate eigenvalues to exact ones, with larger discretization orders, is guaranteed mathematically [7,27].

If a microcavity is shaped as a thinner-than-wavelength flat configuration, then one can reduce the dimensionality of analysis from 3D to 2D in the median plane using the replacement of the refractive index with its effective value [3,5]. This is in agreement to the experimentally found fact that the emission from thin cavities is observed mostly in the cavity plane, its directionality being controlled by the shape of the contour. Such thin flat cavities are commonly called 2D lasers [5]. This and other

review papers [9–11,14,15] provide references for the numerous efforts of researchers to find optimal shapes of the cavity contours. Note that, in practice, the improvement of directionality of emission must be achieved not at the expense of dramatic growth in threshold as it happens with experimentally measured “notched” and “spiral” 2D lasers. Therefore, a LEP can be an attractive instrument in the numerical optimization, which takes account of both the directivity and the threshold of lasing.

So far only spiral and kite-shape microcavity laser modes were studied in [6] and [7] using this approach, where Muller BIE was solved numerically by the Nyström discretization. The kite shape has only one line of mirror symmetry, which was not taken into account in [7]. Still other promising shapes such as ellipse, rectangle, and regular polygons with straight or curved sides can have two, four, and more lines of mirror symmetry. They naturally call for being taken into account.

As LEP is of great interest in the electromagnetic community, we believe that the further development of numerical methods for simulations of resonators with active regions is important. In our ongoing studies, we had noticed that the root-search algorithm stability could be greatly improved if we took into account the symmetry of the studied microcavity; that means, split the solutions to the orthogonal classes of symmetry. Working with determinantal equation of a selected class helps avoid hopping of the code to a nearby eigenvalue belonging to a different class. Besides, this reduces the time for filling in the matrix because the field function and its normal derivative have to be computed only on a part of the whole contour.

Therefore, below we present such an advanced algorithm based on the ideas of [7], but enhanced by taking into account the possible one, two, or four lines of mirror symmetry of the cavity contour. Certain aspects of this algorithm have been published in a contributed conference paper [28]; however, we present here more details and make the corresponding discussion more convincing by presenting additional numerical illustrations.

## 2. FORMULATION AND ANALYTICAL REGULARIZATION OF THE LASING EIGENVALUE PROBLEM

Assume that the electromagnetic field is time-harmonic and choose the time dependence as  $\exp(-ikct)$ , where  $c$  is the light velocity in free space and  $k$  is the wavenumber. Consider the statement of LEP as a boundary-value problem for a generic resonator shown in Fig. 1. This is a dielectric body with the

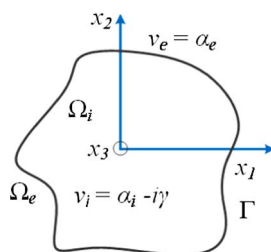


**Fig. 1.** Geometry and notations for a generic 2D uniformly active dielectric microcavity; position vector is  $x = (x_1, x_2)$ .

finite inner domain  $\Omega_i$  bounded with the contour  $\Gamma$  from the infinite outer domain  $\Omega_e$ . It is filled in with a homogeneous nonmagnetic dielectric material that displays gain, i.e., has the known positive real part  $\alpha_i$  and an unknown negative imaginary part  $\gamma$  of the refractive index. By  $\alpha_e$ , we denote the known positive refractive index of the environment  $\Omega_e$ .

We assume that  $\Gamma$  is a twice continuously differentiable curve, and  $n$  is the outer normal unit vector to the boundary  $\Gamma$ . We also denote by  $U$  the space of complex-valued functions, continuous and continuously differentiable curves on  $\bar{\Omega}_i$  and  $\bar{\Omega}_e$ , and twice continuously differentiable on  $\Omega_i$  and  $\Omega_e$ . A non-zero function  $u \in U$  is referred to as an eigenfunction of the LEP corresponding to an eigenvalue pair  $(k_e, \gamma)$  with real components  $k_e > 0$  and  $\gamma > 0$  if the following conditions are satisfied: the Helmholtz equation in each of the domains,

$$\Delta u(x) + k_j^2 u(x) = 0, \quad x \in \Omega_j, \quad j = i, e, \quad (1)$$

the transmission conditions,

$$u^-(x) = u^+(x), \quad \eta_i \frac{\partial u^-(x)}{\partial n(x)} = \eta_e \frac{\partial u^+(x)}{\partial n(x)}, \quad x \in \Gamma, \quad (2)$$

and the Sommerfeld radiation condition at infinity,

$$u(r, \phi) = \sqrt{\frac{2}{i\pi k_e r}} e^{ik_e r} \Phi(\phi), \quad r \rightarrow \infty. \quad (3)$$

Here  $k_j = kv_j$ ;  $\eta_j = \nu_j^{-2}$  in the H-polarization case and  $\eta_j = 1$  in the E-polarization case,  $j = i, e$ ;  $\nu_i = \alpha_i - i\gamma$ ,  $\nu_e = \alpha_e$ ,  $u^+(u^-)$  is the limit value of the function  $u$  from inside (outside) of the boundary  $\Gamma$ ;  $\partial u/\partial n$  is the normal derivative;  $r$  and  $\phi$  are the polar coordinates of the point  $x$ ; and  $\Phi(\phi)$  is the far-field angular emission pattern. Note that as we are interested in the real  $k_e$ , then due to Eq. (3) the lasing mode field does not display exponential growth at infinity.

To build a mathematically convergent algorithm, the boundary-value problem in Eqs. (1)–(3) should be converted to a Fredholm second-kind infinite-matrix equation. To obtain such an equation, we follow [7] and reduce the LEP, in equivalent manner, to the eigenvalue problem for the Muller BIE in terms of two coupled equations:

$$u(x) + \int_{\Gamma} K_{1,1}(x, y) u(y) dl(y) - \int_{\Gamma} K_{1,2}(x, y) v(y) dl(y) = 0, \quad (4)$$

$$v(x) + \int_{\Gamma} K_{2,1}(x, y) u(y) dl(y) - \int_{\Gamma} K_{2,2}(x, y) v(y) dl(y) = 0, \quad (5)$$

where the notation  $v$  is used for the function proportional to the normal derivative of the field function  $u$ , the vectors  $x, y \in \Gamma$ :

$$u(x) = u^-(x) = u^+(x), \quad (6)$$

$$v(x) = \frac{\eta_e + \eta_i \frac{\partial u^+(x)}{\partial n(x)}}{2\eta_i} = \frac{\eta_e + \eta_i \frac{\partial u^-(x)}{\partial n(x)}}{2\eta_e}, \quad (7)$$

$$K_{1,1}(x, y) = \frac{\partial(G_i(x, y) - G_e(x, y))}{\partial n(y)}, \quad (8)$$

$$K_{1,2}(x, y) = \frac{2(\eta_e G_i(x, y) - \eta_i G_e(x, y))}{\eta_e + \eta_i}, \quad (9)$$

$$K_{2,1}(x, y) = \frac{\partial^2 (G_i(x, y) - G_e(x, y))}{\partial n(x) \partial n(y)}, \quad (10)$$

$$K_{2,2}(x, y) = \frac{2}{\eta_e + \eta_i} \frac{\partial(\eta_e G_i(x, y) - \eta_i G_e(x, y))}{\partial n(x)}, \quad (11)$$

and Green's functions of the homogeneous media are the Hankel functions of the first kind and index 0:

$$G_{i/e}(x, y) = \frac{i}{4} H_0^{(1)}(k_{i/e}|x - y|). \quad (12)$$

Note that the functions in Eq. (12) have logarithmic singularities if their arguments coincide and their derivatives are, generally speaking, even more singular. In contrast, the kernel functions in Eqs. (8) and (11), and the function  $K_{1,2}(x, y)$  in the E-polarization case have no singularities (are smooth), and the function  $K_{2,1}(x, y)$  and the function  $K_{1,2}(x, y)$  (in the H-polarization case) have logarithmic singularities (see [5] for the corresponding asymptotic expressions). Thus, the regularization procedure cancels the hyper-order singularities in the IE kernels and their norms are finite in the  $L_2$  sense. This is why Eqs. (4) and (5), collectively, correspond to a Fredholm second-kind operator equation:

$$w + K(\kappa, \gamma)w = 0, \quad (13)$$

where  $w = (u, v)$ . Here, the operator  $K(\kappa, \gamma)$  is generated by the  $2 \times 2$  matrix of the functions  $K_{i,j}(x, y)$ ,  $i, j = 1, 2$ , which depend on the eigenvalue parameter  $(\kappa, \gamma)$ , with  $\kappa$  being the suitably normalized real-valued frequency and  $\gamma$  being the threshold value of the material gain. In laser modeling it is convenient to use  $\kappa$  as a product of the free-space wavenumber  $k_e$  with some linear dimension of the studied cavity. Note that the gain per unit wavelength, frequently met in semiclassical laser theories, can be found as  $g = k\gamma$ . Still we do not use it in our work, as it is convenient only in Fabry–Perot-like cavities.

Inspection of the norm of operator  $K(\kappa, \gamma)$  in the  $L_2$  sense shows that it behaves as  $O(\nu_i^2 - \nu_e^2)$  (see [7]). By this reason, the explained regularization procedure can be called “small-contrast inversion.” As noted in [7], the Muller BIE is free of spurious eigenfrequencies, which infest other, non-Muller, boundary IE types and spoil all based on them numerical algorithms—see details of this topic in [29,30].

Note also that eigenvalue problem in Eq. (13) is somewhat different from more conventional (called “linear”) algebraic eigenvalue problem associated with the equation  $w + \lambda K w = 0$ , where operator  $K$  is independent of the eigenvalue  $\lambda$ . Therefore, it is called a “nonlinear algebraic eigenvalue problem.” Besides, the eigenvalue parameter is not a scalar  $\lambda$  and not a complex number, but a vector of two components,  $(\kappa, \gamma)$ , each of which is a real number.

### 3. NYSTRÖM METHOD DISCRETIZATION WITH ACCOUNT OF SYMMETRY

We propose a new version of the Nyström method of discretization of the Muller IE, based on the account of the presence of one, two, and four axes of symmetry (see Fig. 2) of the cavity

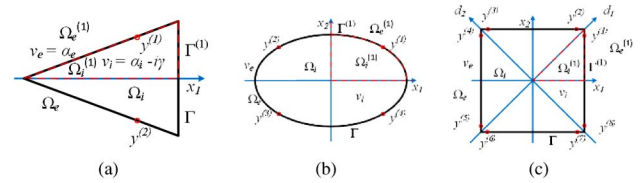


Fig. 2. Geometries of uniformly active 2D microcavities with (a) one, (b) two, and (c) four axes of symmetry.

domain, which is split by these axes into two, four, and eight subdomains.

Thanks to symmetry, we can look for the functions  $w = (u, v)$  as solutions of Eqs. (4) and (5) only on the boundary  $\Gamma^{(1)}$  of the first inner domain  $\Omega_i^{(1)}$  with the corresponding outer domain  $\Omega_e^{(1)}$  (the upper index is the subdomain number). In the other subdomains the field function can be recovered using the symmetry or anti-symmetry conditions. Then the symmetry-adapted Green's functions take the form of

$$G_{i/e}(x, y) = \sum_{p=1}^M c_p F_{i/e}^{(p)}(x, y), \quad (14)$$

where  $M = 2, 4$ , or  $8$ , depending on the number of the axes of symmetry, and coefficients  $c_p$  are given in Tables 1–3 below:

$$F_{i/e}^{(p)}(x, y) = \frac{i}{4} H_0^{(1)}(k_{i/e}|x - y^{(p)}|). \quad (15)$$

We suppose that the boundary curve  $\Gamma$  is defined parametrically as  $r(t) = (r_1(t), r_2(t))$ , where  $t \in [0, 2\pi]$  and  $r_1(t) = f(t) \cos(t)$ ,  $r_2(t) = f(t) \sin(t)$ . As already mentioned in Section 2, one or two (depending on the polarization) of

Table 1. Coefficients  $c_p$  for One Axis of Symmetry

Modes	Notation	$c_1$	$c_2$
$x_1$ -even	$(m, n, e)$	1	1
$x_1$ -odd	$(m, n, o)$	1	-1

Table 2. Coefficients  $c_p$  for Two Axes of Symmetry

Modes	Notation	$c_1$	$c_2$	$c_3$	$c_4$
$x_1$ -even, $x_2$ -even	$(m, n, ee)$	1	1	1	1
$x_1$ -even, $x_2$ -odd	$(m, n, eo)$	1	-1	-1	1
$x_1$ -odd, $x_2$ -odd	$(m, n, oo)$	1	-1	1	-1
$x_1$ -odd, $x_2$ -even	$(m, n, oe)$	1	1	-1	-1

Table 3. Coefficients  $c_p$  for Four Axes of Symmetry

Modes	Notation	$c_1$	$c_2$	$c_3$	$c_4$	$c_5$	$c_6$	$c_7$	$c_8$
$x_1$ -even, $x_2$ -even, $d_1$ -even, $d_2$ -even	$(m, n, eeee)$	1	1	1	1	1	1	1	1
$x_1$ -even, $x_2$ -even, $d_1$ -odd, $d_2$ -odd	$(m, n, eooo)$	1	-1	-1	1	1	-1	-1	1
$x_1$ -odd, $x_2$ -odd, $d_1$ -odd, $d_2$ -odd	$(m, n, oooo)$	1	-1	1	-1	1	-1	1	-1
$x_1$ -odd, $x_2$ -odd, $d_1$ -even, $d_2$ -even	$(m, n, oeee)$	1	1	-1	-1	1	1	-1	-1

the kernel functions  $K$  have logarithmic singularities. Following [7], we extract such a singularity from all four for uniformity:

$$K_{k,l}^{(p)}(t, \tau) = Q_{k,l}^{(p)}(t, \tau) \ln \left( 4 \sin^2 \frac{t - \tau}{2} \right) + P_{k,l}^{(p)}(t, \tau), \tag{16}$$

where  $k, l = 1, 2$ ,

$$Q_{1,1}^{(p)}(t, \tau) = \frac{k_e J_1(k_e |x - y^{(p)}|) - k_i J_1(k_i |x - y^{(p)}|)}{4\pi} \times \frac{((x - y^{(p)}) \cdot n(y^{(p)}))}{|x - y^{(p)}|}, \tag{17}$$

$$Q_{1,2}^{(p)}(t, \tau) = \frac{\eta_i J_0(k_e |x - y^{(p)}|) - \eta_e J_0(k_i |x - y^{(p)}|)}{2\pi(\eta_e + \eta_i)}, \tag{18}$$

$$Q_{2,1}^{(p)}(t, \tau) = \frac{k_i^2 J_2(k_i |x - y^{(p)}|) - k_e^2 J_2(k_e |x - y^{(p)}|)}{4\pi} \times \frac{((x - y^{(p)}) \cdot n(y^{(p)}))((x - y^{(p)}) \cdot n(x))}{|x - y^{(p)}|^2} - \frac{(n(x) \cdot n(y^{(p)}))}{|x - y^{(p)}|} \times \frac{k_i J_1(k_i |x - y^{(p)}|) - k_e J_1(k_e |x - y^{(p)}|)}{4\pi}, \tag{19}$$

$$Q_{2,2}^{(p)}(t, \tau) = \frac{\eta_e k_i J_1(k_i |x - y^{(p)}|) - \eta_i k_e J_1(k_e |x - y^{(p)}|)}{2\pi(\eta_e + \eta_i)} \times \frac{((x - y^{(p)}) \cdot n(x))}{|x - y^{(p)}|}, \tag{20}$$

where  $J_{0,1,2}(\bullet)$  are the Bessel functions and  $P_{k,l}^{(p)}(t, \tau)$  are continuous functions. In computations, we use the trapezoidal rule for the integration of these parts of integrand functions:

$$\int_0^{2\pi/M} g(\tau) d\tau \approx h \sum_{j=0}^{2n} \sigma_j g(t_j), \tag{21}$$

where  $t \in [0, 2\pi/M]$ ,  $h = \pi/(nM)$ ,  $t_j = jh$ ,  $\sigma_j = 1/2$  if  $j = 0$  or  $j = 2n$ , and 1 if  $0 < j < 2n$ . For the logarithmic parts of kernels, we use the quadrature formula for the integration of integrands approximated by trigonometric polynomials:

$$\int_0^{2\pi/M} g(\tau) \ln \left( 4 \sin^2 \frac{t - \tau}{2} \right) d\tau \approx \sum_{j=0}^{2n} \sigma_j R_j^{(M,n)}(t) g(t_j), \tag{22}$$

where

$$R_j^{(M,n)}(t) = -2h \sum_{m=1}^{Mn-1} \frac{\cos(m(t - t_j))}{m} - \frac{h \cos(Mn(t - t_j))}{Mn}. \tag{23}$$

Denote now

$$a_{k,l,j}^{(p)}(t) = R_j^{(p;M,n)}(t) Q_{k,l}^{(p)}(t, t_j) + h P_{k,l}^{(p)}(t, t_j), \tag{24}$$

then

$$\int_{\Gamma} K_{k,l}(x, y) g(y) dI(y) \approx \sum_{j=0}^{2n} \sigma_j \sum_{p=1}^M c_p a_{k,l,j}^{(p)}(t) g(t_j) |r'(t_j)|. \tag{25}$$

Finally, on introducing the notations  $u_i = u(t_i)$ ,  $v_i = v(t_i)$ ,  $a_{k,l,i,j}^{(p)}(t) = a_{k,l,j}^{(p)}(t_i)$ ,  $r'_j = r'(t_j)$ , the unknown values  $u_i$ ,  $v_i$ ,  $i = 0, \dots, 2n$  can be found from the following equations:

$$u_i + \sum_{j=0}^{2n} \sigma_j \sum_{p=1}^M c_p (a_{1,1,i,j}^{(p)} u_j - a_{1,2,i,j}^{(p)} v_j) |r'_j| = 0, \tag{26}$$

$$v_i + \sum_{j=0}^{2n} \sigma_j \sum_{p=1}^M c_p (a_{2,1,i,j}^{(p)} u_j - a_{2,2,i,j}^{(p)} v_j) |r'_j| = 0, \tag{27}$$

with coefficients  $c_p$  given in Tables 1–3 below. Note that in Eqs. (26) and (27) the discretization order is  $n$ , which is the order of the interpolation polynomial in Eq. (23). Now approximate eigenvalues ( $\kappa, \gamma$ ) can be found from the nonlinear algebraic eigenvalue problem:

$$w^{(n)} + K^{(n,n)}(\kappa, \gamma) w^{(n)} = 0, \tag{28}$$

where the eigenvector  $w^{(n)}$  consists of the elements  $u_i$ ,  $v_i$ ,  $i = 0, \dots, 2n$ , while the composition of the entries of the matrix  $K^{(n,n)}$  of order  $2(2n + 1)$  follows from Eqs. (26) and (27).

The solutions of Eq. (28) satisfy a finite-order determinantal equation  $\text{Det}[I^{(n)} + K^{(n,n)}(\kappa, \gamma)] = 0$  and can be found by various numerical methods. Note that the Fredholm property of the Muller IE guarantees the convergence in the sense that larger discretization orders  $n$  entail smaller computational errors, in the  $l_2$ -norm sense (see Appendix A for numerical examples). In our work, we solved this discrete equation by the residual inverse iteration method using the roots found for a circular active cavity as initial guess values.

In concern of the mode field functions, i.e., the LEP eigenfunctions, they have the following symmetry-accounting approximate representations in the domains  $\Omega_i$  and  $\Omega_e$ , respectively, ( $x \in \Omega_{i/e}$ ):

$$u(x) = - \sum_{j=0}^{2n} \sigma_j \sum_{p=1}^M c_p (a_{1,1,j}^{(p)}(x) u_j - a_{1,2,j}^{(p)}(x) v_j) |r'_j|, \tag{29}$$

$$v(x) = - \sum_{j=0}^{2n} \sigma_j \sum_{p=1}^M c_p (a_{2,1,j}^{(p)}(x) u_j - a_{2,2,j}^{(p)}(x) v_j) |r'_j|. \tag{30}$$

### A. Symmetry with Respect to One Axis

Accounting of one axis of symmetry divides the domain  $\Omega_i$  into two parts, and  $M = 2$  [see Fig. 2(a)]. The coefficients  $c_p$  are presented in Table 1, and we use the following notations:

$$y^{(1)} = (y_1, y_2), \quad y^{(2)} = (y_1, -y_2), \tag{31}$$

$$R_{i,j}^{(1;2,n)} = R_{|i-j|}^{(2,n)}, \quad R_{i,j}^{(2;2,n)} = R_{|i+j-2n|}^{(2,n)}, \tag{32}$$

$$R_j^{(2,n)} = R_j^{(2,n)}(0) = -\frac{\pi}{n} \sum_{m=1}^{2n-1} \frac{1}{m} \cos \frac{mj\pi}{2n} - \frac{(-1)^j \pi}{(2n)^2}. \tag{33}$$

**B. Symmetry with Respect to Two Axes**

Accounting of two axes of symmetry divides the domain  $\Omega_i$  into four parts, and  $M = 4$  [see Fig. 2(b)]. The coefficients  $c_p$  are presented in Table 2, and we use the following notations:

$$y^{(1)} = (y_1, y_2), \quad y^{(2)} = (-y_1, y_2), \quad (34)$$

$$y^{(3)} = (-y_1, -y_2), \quad y^{(4)} = (y_1, -y_2), \quad (35)$$

$$R_{ij}^{(1;4,n)} = R_{|i-j|}^{(4,n)}, \quad R_{ij}^{(2;4,n)} = R_{|i+j-4n|}^{(4,n)}, \quad (36)$$

$$R_{ij}^{(3;4,n)} = R_{|i-j-4n|}^{(4,n)}, \quad R_{ij}^{(4;4,n)} = R_{|i+j-8n|}^{(4,n)}, \quad (37)$$

$$R_j^{(4,n)} = R_j^{(4,n)}(0) = -\frac{\pi}{2n} \sum_{m=1}^{4n-1} \frac{1}{m} \cos \frac{mj\pi}{4n} - \frac{(-1)^j \pi}{(4n)^2}. \quad (38)$$

**C. Symmetry with Respect to Four Axes**

Accounting for four axes of symmetry divides the domain  $\Omega_i$  into eight parts, and  $M = 8$  [see Fig. 2(c)]. The coefficients  $c_p$  are presented in Table 3, and we use the following notations:

$$y^{(1)} = (y_1, y_2), \quad y^{(2)} = (y_2, y_1), \quad (39)$$

$$y^{(3)} = (-y_2, y_1), \quad y^{(4)} = (-y_1, y_2), \quad (40)$$

$$y^{(5)} = (-y_1, -y_2), \quad y^{(6)} = (-y_2, -y_1), \quad (41)$$

$$y^{(7)} = (y_2, -y_1), \quad y^{(8)} = (y_1, -y_2), \quad (42)$$

$$R_{ij}^{(1;8,n)} = R_{|i-j|}^{(8,n)}, \quad R_{ij}^{(2;8,n)} = R_{|i+j-4n|}^{(8,n)}, \quad (43)$$

$$R_{ij}^{(3;8,n)} = R_{|i-j-4n|}^{(8,n)}, \quad R_{ij}^{(4;8,n)} = R_{|i+j-8n|}^{(8,n)}, \quad (44)$$

$$R_{ij}^{(5;8,n)} = R_{|i-j-8n|}^{(8,n)}, \quad R_{ij}^{(6;8,n)} = R_{|i+j-12n|}^{(8,n)}, \quad (45)$$

$$R_{ij}^{(7;8,n)} = R_{|i-j-12n|}^{(8,n)}, \quad R_{ij}^{(8;8,n)} = R_{|i+j-16n|}^{(8,n)}, \quad (46)$$

$$R_j^{(8,n)} = R_j^{(8,n)}(0) = -\frac{\pi}{4n} \sum_{m=1}^{8n-1} \frac{1}{m} \cos \frac{mj\pi}{8n} - \frac{(-1)^j \pi}{(8n)^2}. \quad (47)$$

**4. NUMERICAL RESULTS**

In all computations, we assumed that the microcavity material had the refractive index  $\alpha_i = 2.63$  (this is the effective index for a GaAs slab of 200 nm thickness in the infrared range) while the environment was air with  $\alpha_e = 1$  and hence  $k_e = k$ ; we considered only the H-polarized modes because in thin cavities their effective refractive index is significantly larger than for the E-polarized modes.

**A. Elliptic Microcavity Laser**

Figure 3 shows the normalized frequencies of lasing  $\kappa = ka$  and the threshold gains  $\gamma$  for the modes of a uniformly active microcavity shaped as an ellipse with a side ratio  $a/b = 0.5882$ . Here, the symmetry accounting with respect to two axes helps split solutions to four orthogonal classes of the  $x_1$ -even/odd,  $x_2$ -even/odd modes (see Table 2) that contributes to the stability of calculations and reduces the dimensions

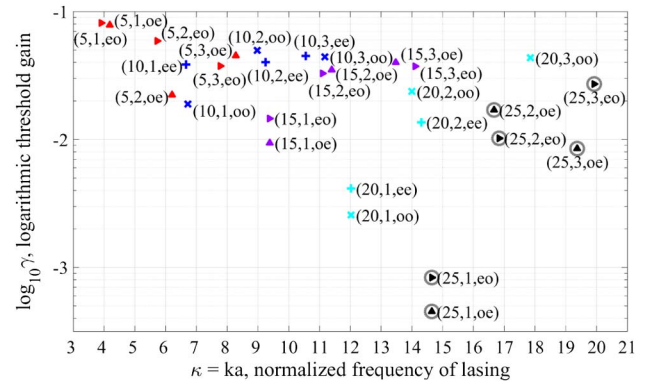


**Fig. 3.** Normalized frequencies of lasing and threshold gains for the active elliptic microcavity laser. Modes  $(m, n, oo)$  are marked with crosses, modes  $(m, n, ee)$  are marked with pluses, modes  $(m, n, eo)$  are marked with right triangles,  $(m, n, oe)$  are marked with top triangles, where  $m$  is the azimuth index and  $n$  is the radial index.

of the finite-dimensional algebraic eigenvalue problem by 4 times.

Mode classification with the aid of indices  $m$  and  $n$  needs special comments. The principles of such classification are clear and unambiguous only in the simplest shapes, like a circle or a square. As the ellipse can be viewed as a result of continuous perturbation of a circle, and keeping in mind that the eigenvalues are also continuous functions of such perturbation, we used, for each mode in the ellipse, the same notations (i.e., indices) as for the eigenvalue-eigenfunction in the circle, from which it was obtained by the contour perturbation. In some cases, this way of assigning the indices keeps correspondence to the actual field pattern—this is so, for instance, for the whispering-gallery modes with radial index of 1 even after their transformation to the modes of an ellipse with considerable eccentricity. In the other cases this principle does not correspond to the actual view of the field pattern—typically this happened to the modes of the circle with higher radial indices. In any case, such a principle of assigning the indices is understandable and reproducible.

Note also that all modes of a perfectly circular cavity with the azimuth index  $m > 0$  are double degenerate, and the transformation of a circle to an ellipse removes this degeneracy. This explains the presence of doublets of modes of the same indices, however of the different symmetries, with respect to the  $x_1$  axis (or  $x_2$  axis) on the plane  $(\kappa, \gamma)$  in Fig. 3. Within any fixed interval of frequencies, the lowest thresholds are observed for the doublets of perturbed whispering-gallery modes with the radial index  $n = 1$ . Interestingly, the frequencies of two modes in each doublet are almost the same; however, the thresholds are sizably different. The lowest thresholds, in each doublet, are always found for the  $x_1$  odd mode. This is understandable because its field has zero values at the longer axis of the ellipse, where the contour curvature is the largest, which entails lower radiation losses.

Figure 4 shows the near- and far-field patterns of three doublets of the H-polarized modes of the elliptic microcavity, indicated in Fig. 3. Note that the modes in panels (a) and (b)

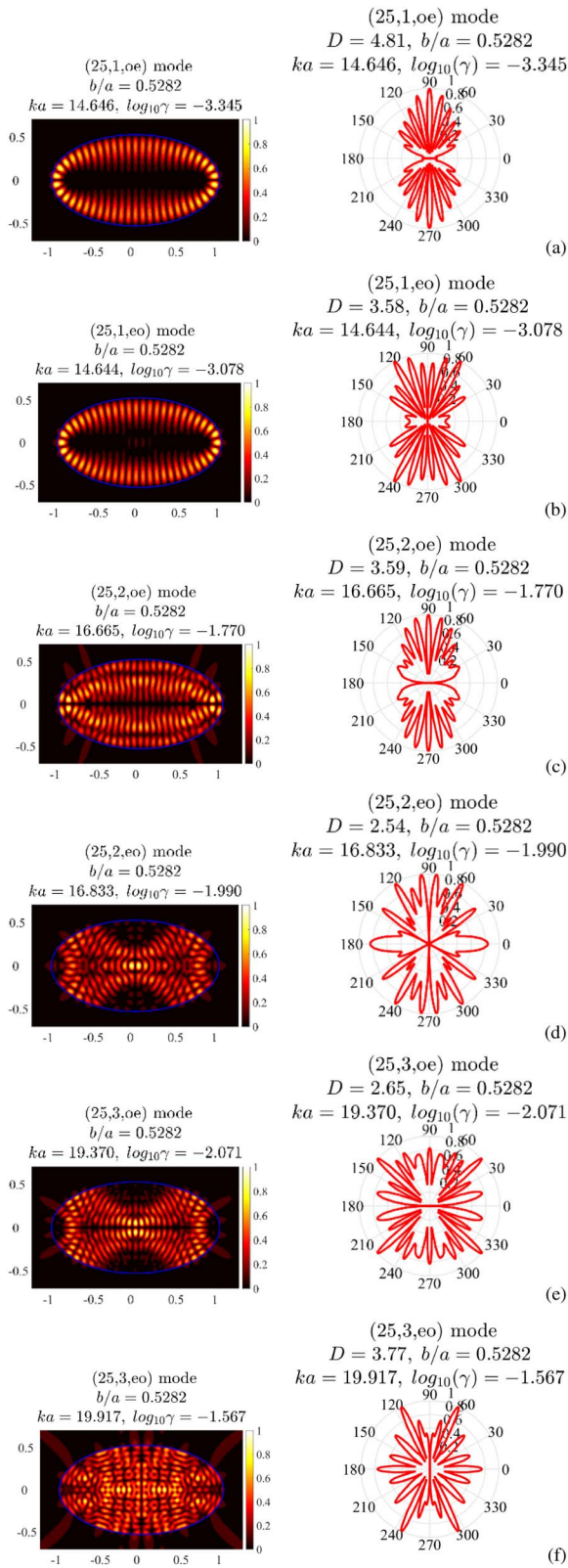


Fig. 4. Modal fields and emission patterns of elliptic microcavity laser.

show features of the whispering-gallery modes, while in panels (d) and (e) show those of the bow-tie modes.

Here the far-field angular pattern  $\Phi(\phi)$  is computed as (see [7])

$$\Phi(\phi) = \int_{\Gamma} \left\{ iu(y)k_e[n(y) \cdot (\cos \phi, \sin \phi)] + \frac{2\eta_i}{\eta_e + \eta_i} v(y) \right\} \times e^{-ik_e(y \cdot (\cos \phi, \sin \phi))} dl(y). \quad (48)$$

The directionality of mode emission can be conveniently characterized using the quantity borrowed from the antenna theory and referred to as directivity:

$$D = 2\pi P^{-1} |\Phi(\phi_{\max})|^2, \quad P = \int_0^{2\pi} |\Phi(\phi)|^2 d\phi, \quad (49)$$

where  $\phi_{\max}$  is the direction of the maximum radiation in the half-space  $0 \leq \phi \leq \pi$  and  $P$  is, within a constant, the total power radiated by a lasing mode. Note that for any mode with index  $m > 0$  of a perfectly circular cavity, the directivity is  $D = 2$ .

## B. Square Microcavity Laser

A uniformly active microcavity shaped as square with the side  $2a$  is an example of a more complicated configuration having as many as four lines of symmetry: middle lines and diagonals. We use a smooth approximation of the square with the aid of “super-circle” characterized by the parametric equations

$$r_1(t) = af(t) \cos t, \quad r_2(t) = af(t) \sin t, \quad (50)$$

$$f(t) = [(\cos t)^{2p} + (\sin t)^{2p}]^{-1/(2p)}, \quad t \in [0, 2\pi], \quad (51)$$

which yield a circle if  $p = 1$  and a square if  $p \rightarrow \infty$ .

Figure 5 shows the normalized frequencies of lasing and the threshold gains for the modes of such a laser. In the mode notation  $(m, n, x)$ , we denote by  $m$  the number of maxima of the mode field along the  $x_1$  side of the square while  $n$  is their number along the  $x_2$  side. In these computations, we took  $p = 10$  that provided the curvature radius of the smoothed corners to be at least 10 times smaller than the free-space wavelength for the modes with  $ka \leq 10$ . As we have found, making  $p$  larger (i.e., making the corners

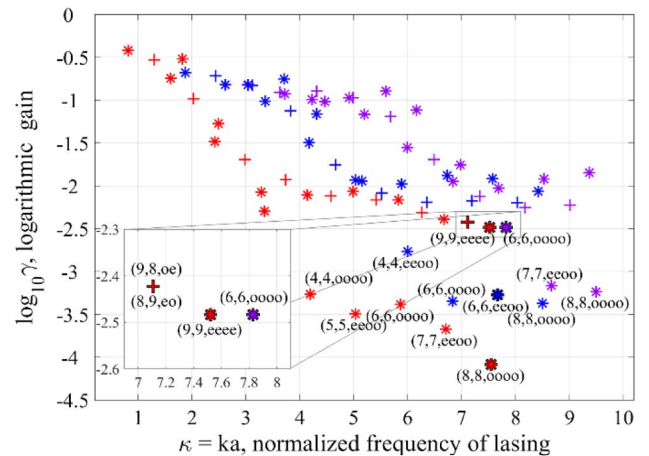
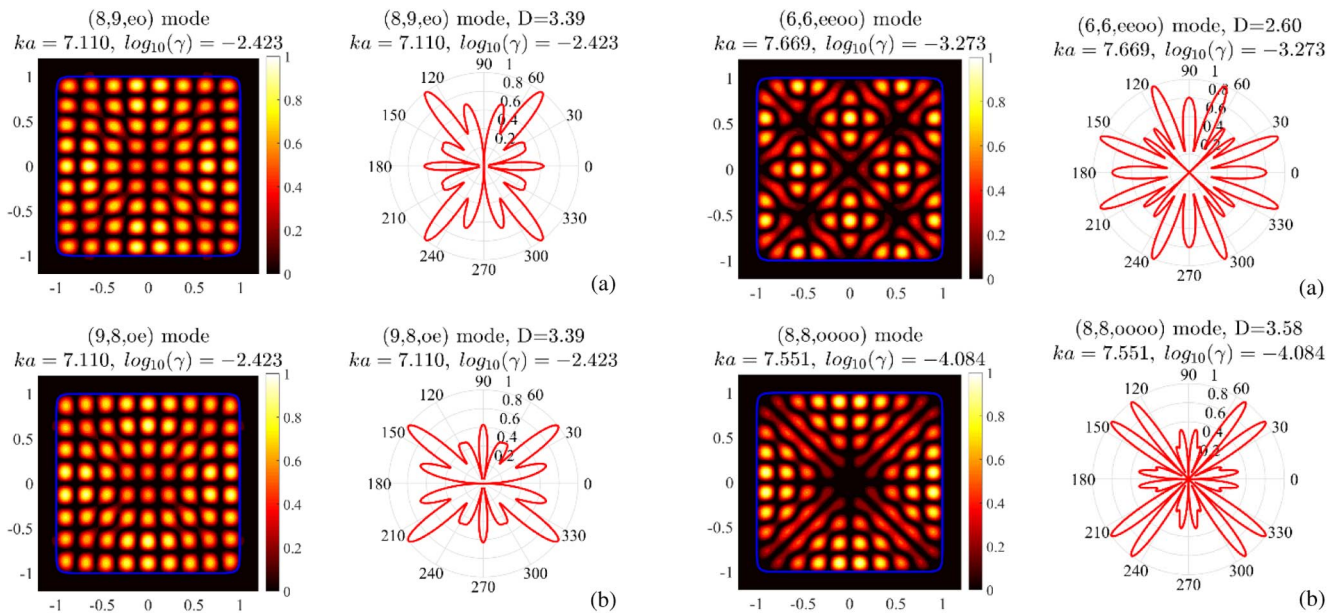


Fig. 5. Normalized frequencies of lasing and threshold gains for the active square microcavity. Modes having symmetry with respect to four axes (see Table 3) are marked with stars; and modes having symmetry with respect to two axes (see Table 2) with crosses.



**Fig. 6.** Square microcavity laser: modal fields and emission patterns having mirror symmetry with respect to two axes.

sharper) resulted in the change of LEP eigenvalues in the fourth digit.

The numbers in the mode notations correspond to the number of bright spots of the mode field along the sides of the square (see Fig. 6). The modes marked with red symbols were obtained by the change in  $p$  from 1 to 10 from the modes of the circle with radial index  $n = 1$  (with blue symbols, from  $n = 2$ ; and with violet symbols, from  $n = 3$ ).

As one can see, the lowest thresholds are associated with the modes which have a high degree of anti-symmetry with respect to the  $x_1$  and  $x_2$  axes and also to the diagonals  $d_1$  and  $d_2$  of the square. These are the modes with indices  $(2m, 2m, oooo)$  and  $(2m + 1, 2m + 1, eooo)$ .

Their reduced thresholds can be explained by the smaller radiation losses than for the other modes that are caused by destructive interference (because of anti-symmetry) of the far fields emitted from different parts of the cavity contour. Besides, the modes with zero fields at the diagonals have lower thresholds because, in this case, the high-curvature corners have a smaller effect on the scattering.

Figures 6 and 7 show the near-field and far-field patterns of the H-polarized modes of the square microcavity having two and four axes of symmetry, respectively. Note that the modal field patterns shown in panels (a) and (b) of Fig. 6 are identical to the rotation by  $90^\circ$ , although they were computed using different determinantal equations. This can serve as additional partial verification of the algorithm.

### 5. CONCLUSION

Account of existing mirror symmetries in the integral-equation analysis of the lasing modes of 2D microcavity lasers leads to the splitting of solutions to orthogonal classes of modes with the corresponding even and odd field symmetries. After that, each class can be computed separately as the roots of

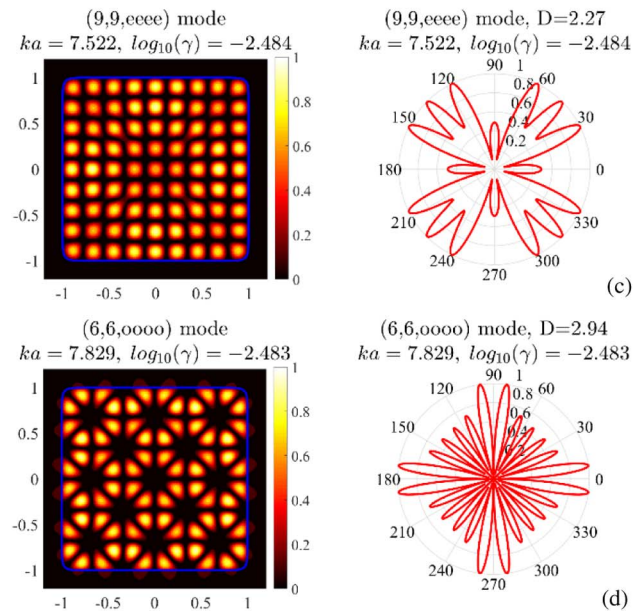


**Fig. 7.** Square microcavity laser: modal fields and emission patterns having mirror symmetry with respect to four axes.

independent determinantal equations. This greatly improves the stability of calculations because iterative root-search algorithms become safe from the hopping to the closely located eigenvalues of different classes of symmetry. We used the Muller BIE in the LEP formulation and presented the details of the Nystrom-type algorithms, which accounted for the field symmetries with respect to one, two, and four lines of symmetry. The power of the modified algorithms was illustrated with numerical examples related to the frequencies, thresholds, and field patterns of the modes of elliptic and square microcavity lasers. The mentioned account of symmetries also reduced the dimensions of the algebraic eigenvalue problem by 2, 4, and 8 times, respectively, which led to considerable saving of the computation time.

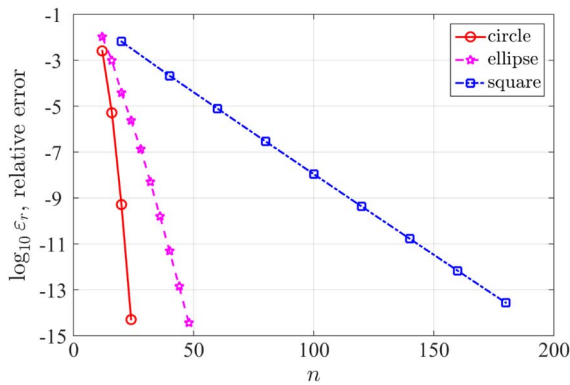


**Fig. 8.** Dependences of computational errors of the LEP eigenvalues on the order of discretization for the cavities shaped as a circle, ellipse, and square. The eigenvalues correspond to the modes obtained as deformation of the mode of the circle with indices (5,1).

## APPENDIX A

The convergence of the meshless Nystrom algorithm applied to discretization of the Muller BIE was grounded mathematically in [7]. It was found that the rate of convergence is exponential with respect to the order of discretization  $n$  (see [7], p. 1736). It is natural that our sophisticated algorithm, which takes account of the lines of symmetry, also shows exponential convergence, if  $n \rightarrow \infty$ . This is demonstrated by the plots in Fig. 8. Here we show the dependences of the relative error, defined as

$$\varepsilon_r = \frac{\|(\kappa_n, \gamma_n) - (\tilde{\kappa}, \tilde{\gamma})\|_2}{\|(\tilde{\kappa}, \tilde{\gamma})\|_2}, \quad (\text{A1})$$

of approximate eigenvalues  $(\kappa_n, \gamma_n)$ , computed for the microcavity lasers with contours shaped as a circle, ellipse and square (super-circle with  $p = 10$ ), on the order of interpolation polynomial  $n$ . As before, we assume that refractive index is  $\alpha_i = 2.63$ . By  $(\tilde{\kappa}, \tilde{\gamma})$ , we denote the approximate eigenvalues computed for the largest used order of the interpolation polynomial. For each point except the starting point, the number of iterations needed to reach the corresponding level of accuracy has to be adapted to that accuracy and varied from 3 to 15.

The plots in Fig. 8 show that the rate of exponential decay of computational error with  $n$  depends on the maximum curvature of the contour involved. The fastest rate is for a circle and it becomes some 8 times smaller if the contour has “edges” smoothed with  $\lambda/10$  rounding, as for the super-circle with  $p = 10$ . Still, in any case, the machine precision is achieved with  $n$  in dozens or small hundreds; this is an achievement beyond any dreams if one uses non-Muller BIE, less-sophisticated discretization, or a rough commercial code.

## REFERENCES

1. S. L. McCall, A. F. J. Levi, R. E. Slusher, S. J. Pearson, and R. A. Logan, “Whispering-gallery mode microdisk lasers,” *Appl. Phys. Lett.* **60**, 289–291 (1992).
2. G. D. Chern, H. E. Tureci, A. Douglas Stone, R. K. Chang, M. Kneissl, and N. M. Johnson, “Unidirectional lasing from InGaN multiple-quantum-well spiral-shaped micropillars,” *Appl. Phys. Lett.* **83**, 1710–1712 (2003).
3. E. I. Smotrova, A. I. Nosich, T. Benson, and P. Sewell, “Cold-cavity thresholds of microdisks with uniform and non-uniform gain:

- quasi-3D modeling with accurate 2D analysis,” *IEEE J. Sel. Top. Quantum Electron.* **11**, 1135–1142 (2005).
4. A. I. Nosich, E. I. Smotrova, S. V. Boriskina, T. M. Benson, and P. Sewell, “Trends in microdisk laser research and linear optical modeling,” *Opt. Quantum Electron.* **39**, 1253–1272 (2007).
5. T. Harayama and S. Shinohara, “Two-dimensional microcavity lasers,” *Laser Photon. Rev.* **5**, 247–271 (2011).
6. E. I. Smotrova, T. M. Benson, P. Sewell, J. Ctyroky, R. Sauleau, and A. I. Nosich, “Optical fields of the lowest modes in a uniformly active thin sub-wavelength spiral microcavity,” *Opt. Lett.* **34**, 3773–3775 (2009).
7. E. I. Smotrova, V. Tsvirkun, I. Gozhyk, C. Lafargue, C. Ulysse, M. Lebental, and A. I. Nosich, “Spectra, thresholds, and modal fields of a kite-shaped microcavity laser,” *J. Opt. Soc. Am. B* **30**, 1732–1742 (2013).
8. L. He, S. K. Ozdemir, and L. Yang, “Whispering gallery microcavity lasers,” *Laser Photon. Rev.* **7**, 60–82 (2013).
9. Y. Zhang, X. Zhang, K. H. Li, Y. F. Cheung, C. Feng, and H. W. Cho, “Advances in III-nitride semiconductor microdisk lasers,” *Phys. Status Solidi A* **212**, 960–973 (2015).
10. S. Yang, Y. Wang, and H. Sun, “Advances and prospects for whispering gallery mode microcavities,” *Adv. Opt. Mater.* **3**, 1136–1162 (2015).
11. H. Cao and J. Wiersig, “Dielectric microcavities: model systems for wave chaos and non-Hermitian physics,” *Rev. Mod. Phys.* **87**, 61–111 (2015).
12. A. S. Zolotukhina, A. O. Spiridonov, E. M. Karchevskii, and A. I. Nosich, “Lasing modes of a microdisk with a ring gain area and of an active microring,” *Opt. Quantum Electron.* **47**, 3883–3891 (2015).
13. A. A. Bogdanov, I. S. Mukhin, N. V. Kryzhanovskaya, M. V. Maximov, Z. F. Sadrieva, M. M. Kulagina, Y. M. Zadiranov, A. A. Lipovskii, E. I. Moiseev, Y. V. Kudashova, and A. E. Zhukov, “Mode selection in InAs quantum dot microdisk lasers using focused ion beam technique,” *Opt. Lett.* **40**, 4022–4025 (2015).
14. X.-F. Jiang, C.-L. Zou, L. Wang, Q. Gong, and Y.-F. Xiao, “Whispering-gallery microcavities with unidirectional laser emission,” *Laser Photon. Rev.* **10**, 40–61 (2016).
15. Y.-D. Yang and Y.-Z. Huang, “Mode characteristics and directional emission for square microcavity lasers,” *J. Phys. D* **49**, 253001 (2016).
16. S. Bittner, C. Lafargue, I. Gozhyk, N. Djellali, L. Milliet, D. T. Hickox-Young, C. Ulysse, D. Bouche, R. Dubertrand, E. Bogomolny, J. Zyss, and M. Lebental, “Origin of emission from square-shaped organic microlasers,” *EPL* **113**, 54002 (2016).
17. S. Nojima, “Theoretical analysis of feedback mechanisms of two-dimensional finite-sized photonic-crystal lasers,” *J. Appl. Phys.* **98**, 043102 (2005).
18. M. P. Nezhad, A. Simic, O. Bondarenko, B. Slutsky, A. Mizrahi, L. Feng, V. Lomakin, and Y. Fainman, “Room-temperature subwavelength metallo-dielectric lasers,” *Nat. Photonics* **4**, 395–399 (2010).
19. A. Mock, “First principles derivation of microcavity semiconductor laser threshold condition and its application to FDTD active cavity modeling,” *J. Opt. Soc. Am. B* **27**, 2262–2272 (2010).
20. S. W. Chang, “Confinement factors and modal volumes of micro- and nanocavities invariant to integration regions,” *IEEE J. Sel. Top. Quantum Electron.* **18**, 1771–1780 (2012).
21. D. Gagnon, J. Dumont, J.-L. Deziel, and L. J. Dube, “Ab initio investigation of lasing thresholds in photonic molecules,” *J. Opt. Soc. Am. B* **31**, 1867–1873 (2014).
22. Y. Huang and Y. Y. Lu, “Efficient method for lasing eigenvalue problems of periodic structures,” *J. Mod. Opt.* **61**, 390–396 (2014).
23. E. I. Smotrova, V. O. Byelobrov, T. M. Benson, J. Ctyroky, R. Sauleau, and A. I. Nosich, “Optical theorem helps understand thresholds of lasing in microcavities with active regions,” *IEEE J. Quantum Electron.* **47**, 20–30 (2011).
24. A. I. Nosich, “Method of analytical regularization in computational photonics,” *Radio Sci.* **51**, 1421–1430 (2016).
25. E. M. Karchevskii and A. I. Nosich, “Methods of analytical regularization in the spectral theory of open waveguides,” in *Proceedings of International Conference on Mathematical Methods in Electromagnetic Theory (MMET)*, Dnipro, Ukraine (2014), pp. 39–45.
26. C. Muller, *Foundations of the Mathematical Theory of Electromagnetic Waves* (Springer, 1969).

27. A. O. Spiridonov and E. M. Karchevskii, "Mathematical and numerical analysis of the spectral characteristics of dielectric microcavities with active regions," in *Proceedings of International Conference Days on Diffraction (DD)*, St. Petersburg, Russia (2016), pp. 390–395.
28. A. O. Spiridonov and E. M. Karchevskii, "Symmetry accounting helps solve the lasing eigenvalue problems for optical microcavities," in *Proceedings of International Conference on Mathematical Methods in Electromagnetic Theory (MMET)*, Lviv, Ukraine (2016), pp. 240–243.
29. A. F. Peterson, "The 'interior resonance' problem associated with surface integral equations of electromagnetics: numerical consequences and a survey of remedies," *Electromagnetics* **10**, 293–312 (1990).
30. S. Amini and S. M. Kirkup, "Solution of Helmholtz equation in the exterior domain by elementary boundary integral methods," *J. Comput. Phys.* **118**, 208–221 (1995).